

Generation of spatial combs digitized by orbital angular momentum

Daniel I. Shahar [ID](#); Havva Begüm Kabagöz [ID](#); Siddharth Ramachandran [ID](#)



APL Photonics 9, 016113 (2024)
<https://doi.org/10.1063/5.0172303>



Articles You May Be Interested In

Multifunctional acoustic holography based on compact acoustic geometric-phase meta-array

J. Appl. Phys. (May 2022)

Review of Scientific Instruments New Products

Rev. Sci. Instrum. (October 2023)

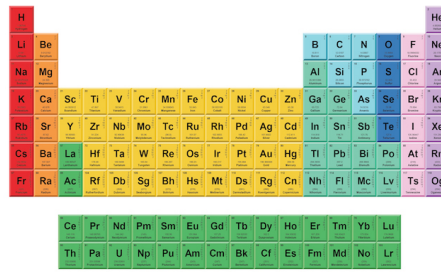
Shaping single photons through multimode optical fibers using mechanical perturbations

APL Photonics (September 2023)



THE MATERIALS SCIENCE MANUFACTURER®

Now Invent.^T



American Elements
Opens a World of Possibilities

...Now Invent!

www.americanelements.com

Generation of spatial combs digitized by orbital angular momentum

Cite as: APL Photon. 9, 016113 (2024); doi: [10.1063/5.0172305](https://doi.org/10.1063/5.0172305)

Submitted: 14 August 2023 • Accepted: 22 December 2023 •

Published Online: 18 January 2024



View Online



Export Citation



CrossMark

Daniel I. Shahar,^{a)}  Havva Begüm Kabagöz,  and Siddharth Ramachandran 

AFFILIATIONS

Boston University, Boston, Massachusetts 02215, USA

^{a)}Author to whom correspondence should be addressed: dshahar@bu.edu

ABSTRACT

Shaping the transverse spatial domain of light has been experiencing recent growth in attention for its applications in optical tweezing, microscopy, communications, and quantum information sciences. The orbital angular momentum (OAM) of light is a transverse physical property that functions as a viable basis for many of such applications. While fields containing a single OAM mode order have extensively been used, fields containing a broad, discrete, and equally spaced OAM spectrum—an OAM comb—has largely been unexplored due to a lack of viable creation methods. Much like how frequency combs enabled myriad applications, it is conceivable that OAM combs would likewise enable further opportunities or expand upon single-OAM applications. For instance, an OAM comb may pave the way for more sophisticated particle manipulation, object detection, and pump shaping for high-dimensional spatial-mode entanglement. Here, we create four OAM combs with rectangular, sinusoidal, sinc, and Gaussian OAM spectral distributions using multiplane light conversion, which only involves phase modulations (hence is inherently lossless) and allows for improved tailoring of the spatial shape. The verification of such combs is done qualitatively by analyzing their propagation evolutions and quantitatively by employing a mode sorting technique—both exhibiting good agreement with user specifications and simulations. The scattering losses of all four combs were measured to be minimal, ranging from 0.66 to 1.04 dB.

© 2024 Author(s). All article content, except where otherwise noted, is licensed under a Creative Commons Attribution (CC BY) license (<http://creativecommons.org/licenses/by/4.0/>). <https://doi.org/10.1063/5.0172305>

INTRODUCTION

The orbital angular momentum (OAM) of light is a physical attribute that has garnered significant attention for its use and promise in a variety of applications, such as classical¹ and quantum communications,² optical tweezers,³ and super-resolution microscopy.⁴ For an electric field, the OAM is attributed to the presence of a helical phase front, $\exp(i\ell\phi)$, where ℓ is the number of phase wraps in the azimuth, ϕ , also known as the topological charge.

The creation of a beam consisting of a single OAM mode is a rather straight-forward procedure, as one need only to modulate the beam with a helical phase of the desired OAM charge. This can be done via readily available tools, such as phase holograms or spatial light modulators (SLMs). However, digitizing the beam's spatial degree of freedom (DoF) through a discrete, equi-spaced OAM spectrum—an OAM comb—remains largely unexplored. Much like how the frequency comb (i.e., the digitization of light's frequency

domain through a broad, discrete, and equi-spaced frequency spectrum) revolutionized technological abilities such as arbitrary waveform generation, ultraprecise metrology, and the study of ultrafast processes,⁵ it is conceivable that its spatial counterpart may likewise pave the way for its own array of applications. For example, Gaussian pumping a $\chi^{(2)}$ nonlinear crystal to generate high-dimensional OAM entanglement⁶ has shortcomings that can be addressed by comb-pumping instead,⁷ such as the generated state's very limited functional form ($(\sum_{\ell} c_{\ell}|-\ell, \ell\rangle)$) and the highly variable, modally dependent production rates. Moreover, as optical tweezers, OAM combs can enhance opportunities to trap particles in more complex structures, such as in three dimensions.⁸ Furthermore, creating OAM combs is paramount to high-dimensional quantum algorithms and protocols that require preparation of superposition states, such as Shor's algorithm⁹ or the quantum secret sharing protocol.¹⁰ Object detection and sensing may also benefit from OAM combs, as probing objects with an OAM comb may reveal

additional information about the object's azimuthal symmetries as compared to the case of a simple Gaussian probe.¹¹ As for classical communications, much as frequency combs with N lines that are wavelength-de-multiplexed and subsequently data-encoded to obtain a compact source that contains N telecommunication wavelength channels covering the bandwidth of optical fibers¹² (thereby obviating the need for N inefficient semiconductor lasers), it is conceivable that an OAM comb could provide similar benefits for spatial multiplexing.

However, the primary reason why OAM combs remain relatively unexplored is the unviability of existing creation methods, of which all employ either amplitude masking^{1,13} or modulation by a single phase plate^{14,15} (or a combination of both¹⁶). Transforming a Gaussian beam into an OAM comb via amplitude masking should be averted because it induces excess loss simply by blocking a significant portion of the beam. Likewise, the application of a single phase plate (e.g., a spiral phase plate with non-integer 2π phase wraps to generate combs with fractional OAM) is also debilitating since the amplitude distribution of an OAM comb is very distinct from a Gaussian beam—a mismatch that a single phase element cannot compensate for. Here, by using a pair of phase plates separated by free space propagation, we demonstrate the creation and characterization of four OAM combs comprising distinct OAM distributions: rectangular (flat), sinusoidal, sinc, and Gaussian. In principle, using two phase plates allows one to achieve full conversion from a Gaussian beam to a desired comb, since the first plate redistributes the beam's amplitude into the comb's amplitude after it has propagated some distance but with a mismatched phase distribution, which then the second plate compensates for. Since the creation process involves only a pair of phase elements, it is theoretically lossless, and experimentally achieved losses ranged between 0.66 and 1.04 dB.

While employing two phase plates separated by free space propagation increases the experimental complexity as compared to a single plate approach, it is merely a minor disadvantage because aligning two diffractive-optic phase-only plates in an optical system is regularly achieved with high fidelity in commercial components such as isolators and wavelength (de)multiplexers.

MODE TRANSFORMATION

The creation of an OAM comb can be achieved by transforming a known input field (typically a Gaussian beam) through a pair of phase plates that are separated by free space propagation, and the phases required to achieve this transformation can be computed *in silico* by an algorithm known as multiplane light conversion¹⁷ (MPLC). MPLC is an inverse-design algorithm that is predominantly used in N-to-N incoherent spatial multiplexers and mode sorters,¹⁸ but here, we show that this algorithm is likewise viable to achieve a 1-to-N coherent transformation (i.e., Gaussian-to-comb). As an inverse-design algorithm, MPLC takes the following inputs: (1) the available incoming field (Gaussian; defined on the first phase plate) and (2) the desired target field (OAM comb; defined on the second phase plate). Note that full complex fields (amplitude and phase) are expected. With both fields defined, MPLC propagates the target field backward to plate 1, where the Gaussian is defined. Plate 1 is then updated to phase-match both fields. The updated plate 1 is applied to the Gaussian beam, which is then propagated forward

to plate 2, followed by updating plate 2 to phase-match both fields. This continuous phase-matching between the two fields at each plate is carried out iteratively until convergence, upon which the resultant phase plates are MPLC's output.

The transverse target field distribution of an OAM comb is determined by constructing a coherent superposition of Laguerre–Gaussian (LG) modes,

$$U_{\text{target}}(r, \phi) = \sum_{p,\ell} c_{p,\ell} LG_{p,\ell}(r, \phi), \quad (1)$$

where

$$LG_{p,\ell}(r, \phi) = N_{p,\ell} \left(\frac{r\sqrt{2}}{w_0} \right)^{|\ell|} \exp \left(-\frac{r^2}{w_0^2} \right) L_p^{|\ell|} \left(\frac{2r^2}{w_0^2} \right) \exp(i\ell\phi) \quad (2)$$

is the LG mode distribution for radial order p and azimuthal order ℓ , w_0 is the beam radius, $L_p^{|\ell|}$ are the generalized Laguerre polynomials, $N_{p,\ell}$ are the normalization constants, and $c_{p,\ell}$ are the user-designed modal weights that define the specific comb. Here, we restrict ourselves to the first-order radial mode $p = 0$ to maintain the equi-spaced nature of the comb and define the OAM spectrum to be the resultant coefficient distribution c_ℓ (although, in principle, one may create fields with higher-order radial modes using the same method).

To demonstrate the versatility of this transformation in tailoring an OAM spectrum, we experimentally create and verify four separate spectral distributions: rectangular, sinusoidal, sinc, and Gaussian. Each distribution comprises different weighting coefficients, $c_\ell (\equiv c_{p=0,\ell})$, given by

$$\begin{aligned} c_\ell^{\text{rect}} &= \frac{1}{\sqrt{N_{\text{rect}}}} \begin{cases} 1, |\ell| \leq 25, \\ 0, |\ell| > 25, \end{cases} & c_\ell^{\text{sin}} &= \frac{1}{\sqrt{N_{\text{sin}}}} \sin\left(\frac{\ell}{10}\right), \\ c_\ell^{\text{sinc}} &= \frac{1}{\sqrt{N_{\text{sinc}}}} \text{sinc}\left(\frac{\ell}{10}\right), & c_\ell^{\text{gauss}} &= \frac{1}{\sqrt{N_{\text{gauss}}}} \exp\left(-\frac{\ell^2}{10^2}\right), \end{aligned} \quad (3)$$

where N_i are the normalization constants determined such that $\sum_i |c_i|^2 = 1$. The 10's appearing in the arguments are user-defined such that sufficient features of the distribution are contained in the modal range $\ell \in [-30, 30]$. In the experimental realizations, the sinusoidal, sinc, and Gaussian distributions are truncated such that $c_\ell = 0$ for $|\ell| > 30$ since power in the OAM spectrum in this range is negligible. In principle, defining complex coefficients is possible, as it would simply yield yet another distinct amplitude and phase distributions for the target field, also achievable by MPLC.

With the OAM spectral distributions under test defined, we construct their amplitude and phase transverse distributions by computing each of the LG modes and summing them up with the distribution's respective weighting factors [Eq. (1)]. Figure 1 illustrates such a construction for the rectangular comb. Evidently, the resultant intensity distribution is concentrated off-center around the $\phi = 0$ azimuth as all the modes are in-phase and hence constructively interfere primarily at this position. In fact, the comb's azimuthal variation is a signature of the Fourier conjugate nature between the azimuthal degree of freedom and the OAM, akin to how a pulse's frequency spectrum is related to its temporal variations. This azimuth–OAM Fourier relation applies insofar as there is a spatial overlap between the modes, which is the case for all radii r

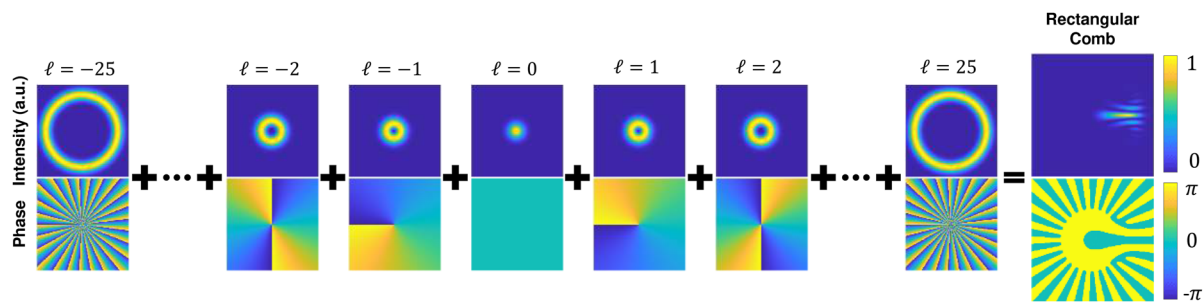


FIG. 1. Construction of the target field of the rectangular comb. All constituent LG modes from $\ell \in [-25, 25]$ are computed and summed with equal weights. The resultant complex field profile is used in the MPLC algorithm for the computation of phase masks.

but the center, although Fourier analyzing the field at a given r yields an OAM spectrum, that is, the total comb's spectrum weighted by the modes' amplitude overlaps. The comb's phase distribution is binary with values 0 or π , indicating that the field is purely real. This is a consequence of the weighting factors' even parity ($c_{-\ell} = c_\ell$) and the fact that LG modes of ℓ and $-\ell$ are complex conjugates (hence their addition is real). Therefore, adding the modes pairwise ($LG_0 + [LG_1 + LG_{-1}] + [LG_2 + LG_{-2}] + \dots + [LG_{25} + LG_{-25}]$) yields a real field.

Choosing $w_0 = 0.5$ mm for the LG basis, the target intensity and phase profiles for all combs under test are shown in Fig. 2. Like the rectangular comb, the sinc and Gaussian combs are purely

real due to their modal weights' even parity. However, the sinusoidal comb is constructed out of modal weights with odd parity ($c_{-\ell} = -c_\ell$), which results in a purely imaginary field profile, as evident by its binary phase of $\pm\pi/2$. With an input Gaussian of beam radius $w_0^{in} = 0.885$ mm at a wavelength of 1550 nm and two phase plates separated by 115 mm of free space, the MPLC-obtained phase masks, which are computed in MATLAB,^{18,19} for each of the combs are shown in the right two columns of Fig. 2. Prior to the phase mask computation, the target field profiles are shifted leftward by 1.2125 mm (97 pixels) to obtain convergent solutions with smoother phase masks. The phase masks improve with the shifting because, otherwise, lateral translation of the field is necessary in addition to

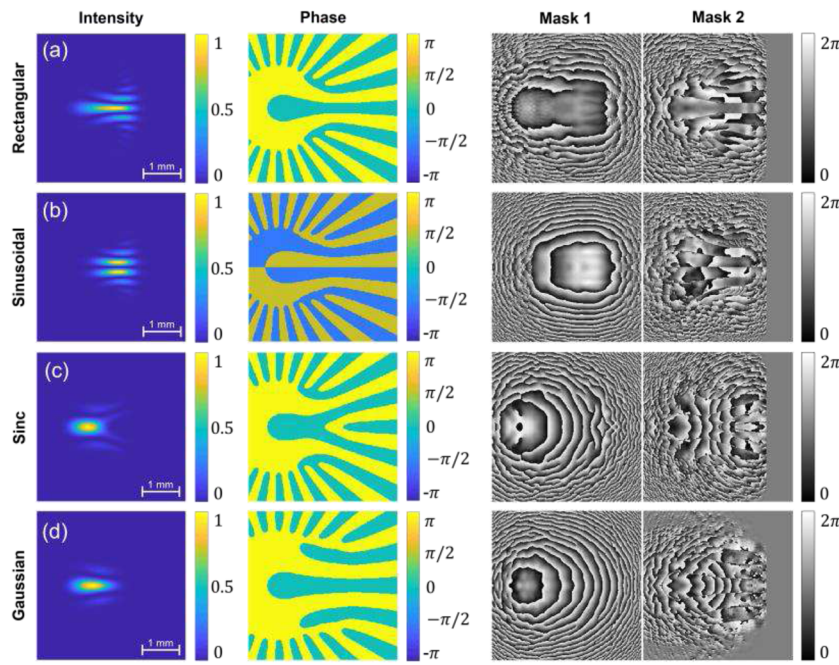


FIG. 2. Left two columns: the intensity and phase profiles for the (a) rectangular, (b) sinusoidal, (c) sinc, and (d) Gaussian combs. Right two columns: MPLC-obtained phase masks necessary to perform transformation. The input Gaussian size used is $w_0^{in} = 0.885$ mm, and the free-space separation between the masks is 115 mm.

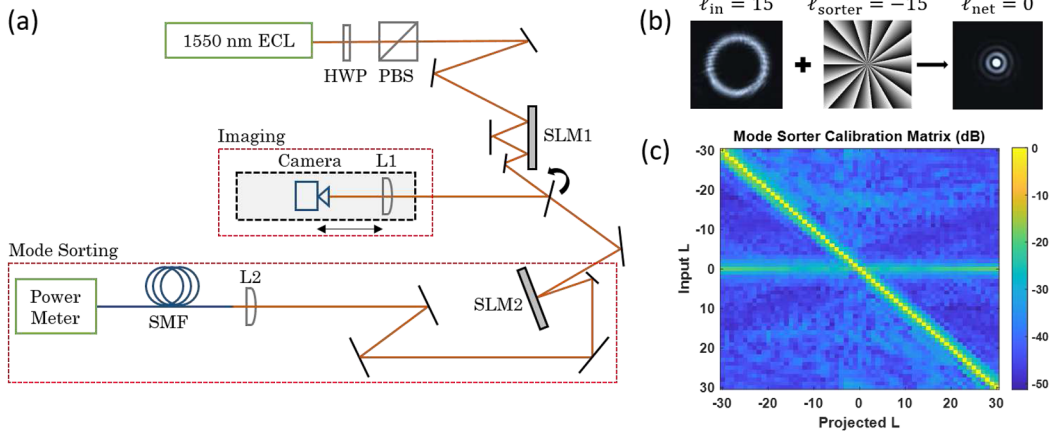


FIG. 3. (a) Experimental setup. Light from a 1550 nm ECL, transmitted through a HWP and a PBS, is configured to bounce twice off SLM1 to create the comb. Its characterization is done qualitatively (imaging) and quantitatively (mode sorting). The imaging system comprises an InGaAs camera and an imaging lens (L1)—both mounted on a translational rail. The mode sorting system includes a sorting SLM (SLM2) followed by a coupling lens (L2), an SMF, and a powermeter. (b) Applying the opposite helical phase ($\ell_{\text{sorter}} = -15$) transforms an LG mode ($\ell_{\text{in}} = 15$) to a Bessel mode ($\ell_{\text{net}} = 0$) in the far field. (c) Calibration matrix of the mode sorter, with each row normalized by the input power of the LG mode before SLM2. For illustration, the main diagonal is equalized row-by-row to 0 dB.

it shaping into the desired comb, i.e., the masks would incur phase components akin to a linear diffraction grating, which would complicate their structure and decrease the operational bandwidth. By simulating the Gaussian's propagation through the resultant phase plates, we obtain overlaps of 98.9% (rectangular), 98.8% (sinusoidal), 99.5% (sinc), and 99.5% (Gaussian).

EXPERIMENTAL SETUP

The experimental setup (Fig. 3) comprises a 1550 nm external cavity laser (ECL; New Focus 6528-LN) input source and a spatial light modulator (SLM1; Hamamatsu X13138; 1024 × 1272 pixels; 12.5 μm pixel size) that is sectioned into two. Each section corresponds to the application of a separate phase mask. The input Gaussian beam ($w_0 = 0.885$ mm) is imaged onto the first phase mask and is aligned such that it bounces off the center of both masks. The bounce mirror is positioned such that the total propagation distance between the two masks is 115 mm, and the desired target field is defined at the second mask immediately upon its application. A combination of a half-wave plate (HWP) and a polarizing beam splitter (PBS) polarizes the beam to match the SLM's liquid crystal modulation axis and provides power control by adjusting the HWP angle.

The converted beam, or comb, at the output is characterized in two ways. First, we send it to a camera-lens system that images the light at the second SLM plane onto the camera (Allied Vision Gold-eye G-033 TECless). This provides a qualitative confirmation of the intensity distribution. Furthermore, the system is positioned on a translational rail, allowing for the imaging of the comb at arbitrary, but measurable, propagation distances. Comparing the experimental propagated intensity distributions with the simulations qualitatively confirms that not only the intensity profile matches well on the

second plane but also the phase profile matches (as both intensity and phase affect the evolution of a beam).

To quantitatively measure its OAM spectrum, the comb is sent to a mode sorting system. This system comprises an additional SLM (SLM2; Santec SLM-200; 1200 × 1920 pixels; 8 μm pixel size) followed by coupling into a single-mode fiber (SMF) and a power readout. To measure the power at a given mode ℓ_m , we project a helical phase pattern of opposite OAM $-\ell_m$ onto SLM2. This converts the desired component to-be-measured to contain no net OAM ($\Delta\ell = 0$) and, hence, results in non-zero coupling into the SMF. All the other modes that do not match the opposite helical projection are filtered out by the SMF as they contain a non-zero net OAM. This projection is performed for all $\ell \in [-30, 30]$, which yields the beam's measured OAM spectrum in this range.

The calibration of the mode sorter is carried out by creating, likewise via MPLC, the constituent LG modes at the second plane and subjecting them to the same projective measurements as the combs under test. When an LG mode is projected with its opposite helical phase, it is converted to a Bessel beam at far-field [Fig. 3(b)]. This produces a near-diagonal 61-by-61 transmission matrix, as shown in Fig. 3(c), that is inverted and applied to each of the measured comb distributions. The mode sorter can measure parasitic modal power down to at least -20 dB, as is evident from the off-diagonal to on-diagonal extinction ratios for all the modes. The near-constant power measured in the $\ell_{\text{input}} = 0$ row is attributed to SLM2's imperfect conversion efficiency, i.e., a fraction of the incident power does not experience the phase modulation. Therefore, when $\ell = 0$ is incident, a portion of the $\ell = 0$ unconverted power successfully couples into the SMF. This is not the case when $\ell \neq 0$ is incident, as the unconverted power remains with a helical phase and is subsequently rejected by the SMF.

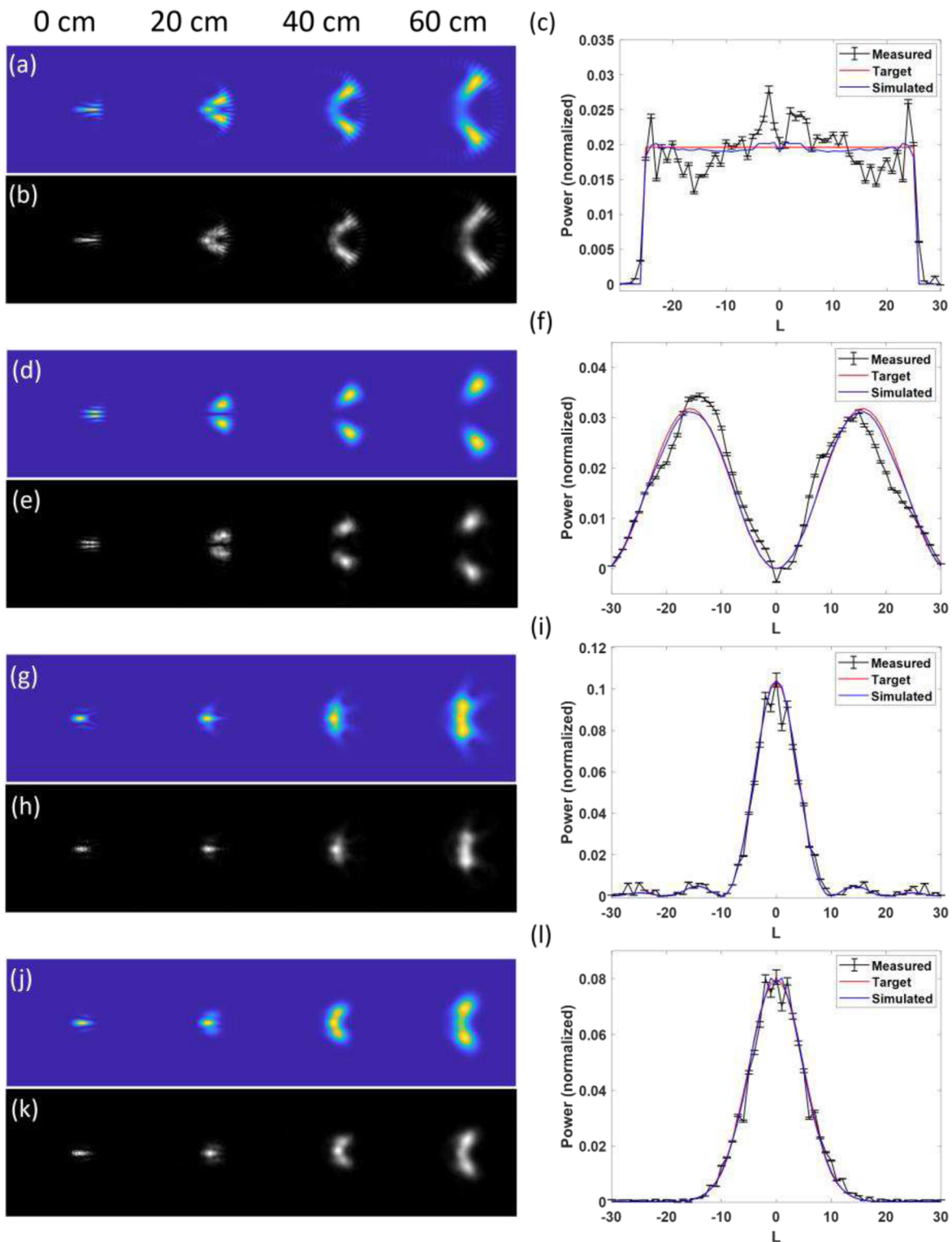


FIG. 4. Experimental results. (a) and (b) Simulated and measured propagation evolution of the rectangular comb every 20 cm, showing a good match between simulations and experiments, and representative image bifurcation upon propagation, resulting from the angular momentum dependence of Gouy phase. (c) Measured (black), target (red), and simulated (blue) OAM spectra of the rectangular comb. Respective results for the sinusoidal (d)–(f), sinc (g)–(i), and Gaussian (j)–(l) combs.

RESULTS

The qualitative and quantitative results are summarized in Fig. 4. For each of the four combs, the top bar represents its simulated propagation evolution from the second phase mask ($z = 0$) to $z = 60$ cm in steps of 20 cm and the bottom bar shows the corresponding images taken at such positions. As seen, the measured beam pattern evolutions closely match the simulations for all four combs. Furthermore, with propagation, the beam pattern of each comb spectrum bifurcates into two separate arms, which is most clearly evident for the rectangular comb [Figs. 4(a) and 4(b)]. This is understood by considering the influence of the sign of ℓ of the components that comprise the comb on free-space propagation. In general, rotating a field by an angle α in the transverse plane is equivalent to multiplying the phase factor $\exp(i\alpha\ell)$ to each of its constituent LG modes,²⁰

$$\sum_{\ell} c_{\ell} LG_{0,\ell}(r, \phi) \rightarrow \sum_{\ell} c_{\ell} LG_{0,\ell}(r, \phi) \exp(i\alpha\ell). \quad (4)$$

Explicitly, the comb at its beam waist ($z = 0$, second SLM plane) can be decomposed as

$$\begin{aligned} U(r, \phi; 0) &= \sum_{\ell} c_{\ell} LG_{0,\ell}(r, \phi; 0) \\ &= \sum_{\ell} c_{\ell} N_{0,\ell} \left(\frac{r\sqrt{2}}{w_0} \right)^{|\ell|} \exp\left(-\frac{r^2}{w_0^2}\right) \exp(i\ell\phi). \end{aligned} \quad (5)$$

As the field propagates, each constituent LG mode transforms as

$$\begin{aligned} LG_{0,\ell}(r, \phi; 0) &\rightarrow LG_{0,\ell}(r, \phi; z) \\ &= N_{0,\ell} \left(\frac{r\sqrt{2}}{w(z)} \right)^{|\ell|} \exp\left(-\frac{r^2}{w^2(z)}\right) \\ &\quad \times \exp\left(-ik\frac{r^2}{2R(z)}\right) \exp(i\psi_{\ell}(z)) \exp(i\ell\phi), \end{aligned} \quad (6)$$

where $w(z) = w_0\sqrt{1 + (z/z_R)^2}$ is the expanded beam waist, $R(z) = z[1 + (z_R/z)^2]$ is the phase front's radius of curvature, $\psi_{\ell}(z) = (1 + |\ell|)\text{atan}(z/z_R)$ is the Gouy phase acquired by mode ℓ , and $z_R = \pi w_0^2/\lambda$ is the beam's Rayleigh range. Therefore, the comb at z can be written as

$$\begin{aligned} U(r, \phi; z) &= \sum_{\ell} c_{\ell} LG_{0,\ell}(r, \phi; z) \\ &= \sum_{\ell} \left[c_{\ell} N_{0,\ell} \left(\frac{r\sqrt{2}}{w(z)} \right)^{|\ell|} \exp\left(-\frac{r^2}{w^2(z)}\right) \right. \\ &\quad \times \exp\left(-ik\frac{r^2}{2R(z)}\right) \exp\left(i\text{atan}\frac{z}{z_R}\right) \exp(i\ell\phi) \\ &\quad \left. \times \exp\left(i|\ell|\text{atan}\frac{z}{z_R}\right) \right]. \end{aligned} \quad (7)$$

For $\ell > 0$, each mode acquires an ℓ -dependent longitudinal phase of $\ell \text{atan}(z/z_R)$, resulting in a rotation of angle $\alpha(z) = \text{atan}(z/z_R)$ (in addition to diffractive effects), whereas for $\ell < 0$, the ℓ -dependent longitudinal phase is $-\ell \text{atan}(z/z_R)$, resulting in an

TABLE I. Estimated scattering losses attributed to the generation of each comb with respect to the input Gaussian beam and obtained by measuring the total loss through SLM1 and adjusting by its material loss.

Distribution	Scattering loss (dB)
Rectangular	0.66
Sinusoidal	0.86
Sinc	1.04
Gaussian	0.96

angle of $-\alpha(z)$. This entails that the bifurcation is a consequence of the $|\ell|$ dependence of the Gouy phase rather than ℓ .

The measured OAM spectrum of the rectangular comb is shown in Fig. 4(c) (black curve), and it is compared with the target spectrum (red curve) and the simulated spectrum (blue curve). The relative standard deviation, which is a metric quantifying the distribution's flatness, is calculated to be 16.7% in the interval $\ell \in [-25, 25]$. The respective results for the sinusoidal distribution, sinc distribution, and Gaussian distribution are shown in Figs. 4(f), 4(i), and 4(l), of which all match well with their target fields. The error bars are due to power fluctuations during measurement.

Finally, the scattering losses attributed to the phase masks were estimated by measuring the output power of the comb relative to the input power of the Gaussian followed by subtracting 1.64 dB, the material loss of SLM1, measured analogously with blank phase masks. The losses are summarized in Table I.

SUMMARY AND CONCLUSIONS

We experimentally demonstrate the capability of transforming a Gaussian beam into a complex field comprising a tailored and broad OAM spectral distribution, or comb, using only a pair of phase plates. The usage of phase elements only renders this technique theoretically lossless and with experimental losses lower than 1.04 dB. In addition to low loss, this structure grants versatility by allowing one to create a target field with arbitrary amplitude and phase, and we show that multiplane light conversion (MPLC) can be used to obtain the required phase plate profiles. The versatility of the creation method is verified by independently producing and confirming four separate OAM spectral distributions: rectangular, sinusoidal, sinc, and Gaussian. Each of such combs is shown to exhibit unique propagation properties, such as bifurcation and Gouy-phase-enabled rotation. The versatile production and control of a digital spatial comb through its OAM spectrum will pave the way for numerous applications in particle manipulation, object detection, classical and quantum communications, pump shaping, and high-dimensional entanglement.

ACKNOWLEDGMENTS

The authors thank X. Liu, A. Peterson-Greenberg, and Z. Ma for their insightful discussions and A. McCall for help with instrumentation. This work was supported by the Vannevar Bush Faculty Fellowship (Grant No. N00014-19-1-2632), the Multi-University Research Initiative (MURI) (Grant No. N00014-20-1-2450), and

the National Science Foundation Graduate Research Fellowship (NSF-GRF) (Grant No. 2234657).

AUTHOR DECLARATIONS

Conflict of Interest

The authors have no conflicts to disclose.

Author Contributions

Daniel I. Shahar: Conceptualization (equal); Data curation (lead); Formal analysis (equal); Investigation (lead); Methodology (equal); Software (lead); Validation (lead); Visualization (lead); Writing – original draft (equal); Writing – review & editing (equal). **Havva Begüm Kabagöz:** Methodology (equal); Writing – review & editing (equal). **Siddharth Ramachandran:** Conceptualization (equal); Formal analysis (equal); Funding acquisition (lead); Methodology (equal); Project administration (lead); Resources (lead); Supervision (lead); Writing – original draft (equal); Writing – review & editing (equal).

DATA AVAILABILITY

The data that support the findings of this study are available from the corresponding author upon reasonable request.

REFERENCES

- ¹J. Wang, J. Yang, I. M. Fazal, N. Ahmed, Y. Yan, H. Huang, Y. Ren, Y. Yue, S. Dolinar, M. Tur, and A. E. Willner, “Terabit free-space data transmission employing orbital angular momentum multiplexing,” *Nat. Photonics* **6**, 488 (2012).
- ²A. Mair, A. Vaziri, G. Weihs, and A. Zeilinger, “Entanglement of the orbital angular momentum states of photons,” *Nature* **412**, 313 (2001).
- ³H. He, M. E. J. Friese, N. R. Heckenberg, and H. Rubinsztein-Dunlop, “Direct observation of transfer of angular momentum to absorptive particles from a laser beam with a phase singularity,” *Phys. Rev. Lett.* **75**(5), 826 (1995).
- ⁴S. W. Hell and J. Wichmann, “Breaking the diffraction resolution limit by stimulated emission: Stimulated-emission-depletion fluorescence microscopy,” *Opt. Lett.* **19**(11), 780 (1994).
- ⁵T. Fortier and E. Baumann, “20 years of developments in optical frequency comb technology and applications,” *Commun. Phys.* **2**, 153 (2019).
- ⁶A. C. Dada, J. Leach, G. S. Buller, M. J. Padgett, and E. Andersson, “Experimental high-dimensional two-photon entanglement and violations of generalized Bell inequalities,” *Nat. Phys.* **7**, 677 (2011).
- ⁷E. V. Kovlakov, S. S. Straupe, and S. P. Kulik, “Quantum state engineering with twisted photons via adaptive shaping of the pump beam,” *Phys. Rev. A* **98**, 060301(R) (2018).
- ⁸M. P. MacDonald, L. Paterson, K. Volke-Sepulveda, J. Arlt, W. Sibbett, and K. Dholakia, “Creation and manipulation of three-dimensional optically trapped structures,” *Science* **296**, 1101 (2002).
- ⁹P. W. Shor, “Algorithms for quantum computation: Discrete logarithms and factoring,” in *Proceedings 35th Annual Symposium on Foundations of Computer Science* (IEEE, 1994), p. 124.
- ¹⁰J. Pinnell, I. Nape, M. de Oliveira, N. Tabebordbar, and A. Forbes, “Experimental demonstration of 11-dimensional 10-party quantum secret sharing,” *Laser Photonics Rev.* **14**, 2000012 (2020).
- ¹¹G. Xie, H. Song, Z. Zhao, G. Milione, Y. Ren, C. Liu, R. Zhang, C. Bao, L. Li, Z. Wang, K. Pang, D. Starodubov, B. Lynn, M. Tur, and A. E. Willner, “Using a complex optical orbital-angular-momentum spectrum to measure object parameters,” *Opt. Lett.* **42**(21), 4482 (2017).
- ¹²K. Ingerslev, P. Gregg, M. Galili, F. Da Ros, H. Hu, F. Bao, M. A. Usuga Castaneda, P. Kristensen, A. Rubano, L. Marrucci, K. Rottwitt, T. Morioka, S. Ramachandran, and L. K. Oxenløwe, “12 mode, WDM, MIMO-free orbital angular momentum transmission,” *Opt. Express* **26**, 20225 (2018).
- ¹³Y. Yang, Q. Zhao, L. Liu, Y. Liu, C. Rosales-Guzmán, and C. Qiu, “Manipulation of orbital-angular-momentum spectrum using pinhole plates,” *Phys. Rev. Appl.* **12**, 064007 (2019).
- ¹⁴E. Bolduc, N. Bent, E. Santamato, E. Karimi, and R. W. Boyd, “Exact solution to simultaneous intensity and phase encryption with a single phase-only hologram,” *Opt. Lett.* **38**, 3546 (2013).
- ¹⁵G. Yang, B. Dong, B. Gu, J. Zhuang, and O. K. Ersoy, “Gerchberg–Saxton and Yang–Gu algorithms for phase retrieval in a nonunitary transform system: A comparison,” *Appl. Opt.* **33**, 209 (1994).
- ¹⁶J. Pinnell, V. Rodríguez-Fajardo, and A. Forbes, “Single-step shaping of the orbital angular momentum spectrum of light,” *Opt. Express* **27**, 28009 (2019).
- ¹⁷G. Labroille, B. Denolle, P. Jian, P. Genevaux, N. Treps, and J.-F. Morizur, “Efficient and mode selective spatial mode multiplexer based on multi-plane light conversion,” *Opt. Express* **22**, 15599 (2014).
- ¹⁸N. K. Fontaine, R. Ryf, H. Chen, D. T. Neilson, K. Kim, and J. Carpenter, “Laguerre–Gaussian mode sorter,” *Nat. Commun.* **10**, 1865 (2019).
- ¹⁹D. Shahar and S. Ramachandran, “Generation of spatial combs digitized by orbital angular momentum,” in CLEO SW4F.3, 2022.
- ²⁰F. Li, T. Xu, W. Zhang, X. Qiu, X. Lu, and L. Chen, “Optical images rotation and reflection with engineered orbital angular momentum spectrum,” *Appl. Phys. Lett.* **113**, 161109 (2018).